Quadrotor Helicopter Flight Dynamics and Control: Theory and Experiment

4 authors, including:

Gabriel Hoffmann
Zee.Aero
28 PUBLICATIONS   8,364 CITATIONS

SEE PROFILE

Steven L. Waslander
University of Waterloo
196 PUBLICATIONS   10,311 CITATIONS

SEE PROFILE

Quadrotor Helicopter Flight Dynamics and Control: Theory and Experiment[*]

Gabriel M. Hoffmann[†]   Haomiao Huang[‡]   Steven L. Waslander[§]   Claire J. Tomlin [¶]

   Quadrotor helicopters are emerging as a popular platform for unmanned aerial vehicle (UAV) research, due to the simplicity of their construction and maintenance, their ability to hover, and their vertical take off and landing (VTOL) capability. Current designs have often considered only nominal operating conditions for vehicle control design. This work seeks to address issues that arise when deviating significantly from the hover flight regime. Aided by well established research for helicopter flight control, three separate aerodynamic effects are investigated as they pertain to quadrotor flight, due to vehicular velocity, angle of attack, and airframe design. They cause moments that affect attitude control, and thrust variation that affects altitude control. Where possible, a theoretical development is first presented, and is then validated through both thrust test stand measurements and vehicle flight tests using the Stanford Testbed of Autonomous Rotorcraft for Multi-Agent Control (STARMAC) quadrotor helicopter. The results enabled improved controller performance.

I.   Introduction

   Quadrotor helicopters are an emerging rotorcraft concept for unmanned aerial vehicle (UAV) platforms. The vehicle consists of four rotors in total, with two pairs of counter-rotating, fixed-pitch blades located at the four corners of the aircraft, an example of which is shown in Figure 1. Due to its specific capabilities, use of autonomous quadrotor vehicles has been envisaged for a variety of applications both as individual vehicles and in multiple vehicle teams, including surveillance, search and rescue and mobile sensor networks.[1]

   The particular interest of the research community in the quadrotor design can be linked to two main advantages over comparable vertical take off and landing (VTOL) UAVs, such as helicopters. First, quadrotors do not require complex mechanical control linkages for rotor actuation, relying instead on fixed pitch rotors and using variation in motor speed for vehicle control. This simplifies both the design and maintenance of the vehicle. Second, the use of four rotors ensures that individual rotors are smaller in diameter than the equivalent main rotor on a helicopter, relative to the airframe size. The individual rotors, therefore, store less kinetic energy during flight, mitigating the risk posed by the rotors should they entrain any objects. Furthermore, by enclosing the rotors within a frame, the rotors can be protected from breaking during collisions, permitting flights indoors and in obstacle-dense environments, with low risk of damaging the vehicle, its operators, or its surroundings. These added safety benefits greatly accelerate the design and test flight process by allowing testing to take place indoors, by inexperienced pilots, with a short turnaround time for recovery from incidents.

American Institute of Aeronautics and Astronautics

Figure 1. STARMAC II quadrotor aircraft unmanned aerial vehicle (UAV), in flight, with autonomous attitude and altitude control. This is a vehicle of the Stanford Testbed of Autonomous Rotorcraft for Multi-Agent Control (STARMAC) project. Applications include search and rescue, surveillance operation in cluttered environments, and mobile sensor networks. Operation throughout the flight envelope allows characterization of the aerodynamic disturbance effects on the control system, caused by vehicle motion relative to the free stream. The reconfigurable airframe allows the effect of structures near the rotor slip streams to be examined.

Previous treatments of quadrotor vehicle dynamics have often ignored known aerodynamic effects of rotorcraft vehicles. At slow velocities, such as while hovering, this is indeed a reasonable assumption. However, even at moderate velocities, the impact of the aerodynamic effects resulting from variation in air speed is significant. Although many of the effects have been discussed in the helicopter literature,[2–5] their influence on quadrotors has not been comprehensively explored. This work focuses on three aerodynamic effects experienced by quadrotors, one that impacts altitude control and two that impact attitude control. First, for altitude control, total thrust is affected by the vehicle velocity and by the angle of attack, with respect to the free stream. This nonlinear function consists of three nonlinear flight regimes, one of which results in a stochastic thrust profile. Second, for attitude control, advancing and retreating blades experience differing inflow velocities, resulting in a phenomenon called blade flapping. This induces roll and pitch moments at the blade root, and tips the thrust vector away from the horizontal plane. Finally, interference caused by the various components of the vehicle body, near the rotor slipstream, causes unsteady thrust behavior and poor attitude tracking. This interference was demonstrated to be significantly influenced by airframe modifications. For all but the last effect, a theoretical derivation is developed based on previous work on rotorcraft, and the specific impact on quadrotor dynamics is developed. All effects are then validated through thrust test stand experiments and flight tests, using the Stanford Testbed of Autonomous Rotorcraft for Multi-Agent Control (STARMAC).

We proceed with a brief survey of development efforts for quadrotor vehicles in Section II. Section III presents details of the test stand apparatus and the STARMAC II testbed, and the nonlinear vehicle dynamics for quadrotors are then summarized in Section IV. In Section V, we present analysis of each of the aerodynamic effects as they pertain to quadrotor vehicles, along with experimental results demonstrating their presence in thrust test stand experiments. In Section VI, results from indoor and outdoor flight tests are presented, with an analysis of the impact of the aerodynamic effects. Finally, flight results for outdoor hover control are presented.

II. Background

Although the first successful quadrotors flew in the 1920's,[4] no practical quadrotor helicopters have been built until recently, largely due to the difficulty of controlling four motors simultaneously with sufficient bandwidth. The only manned quadrotor helicopter to leave ground effect was the Curtiss-Wright X-19A in 1963, though it lacked a stability augmentation system to reduce pilot work load, rendering stationary hover

American Institute of Aeronautics and Astronautics

near impossible,[6] and development stopped at the prototype stage. Recently, advances in microprocessor capabilities and in micro-electro-mechanical-system (MEMS) inertial sensors have spawned a series of radio-controlled (RC) quadrotor toys, such as the Roswell flyer (HMX-4),[7] and Draganflyer,[8] which include stability augmentation systems to make flight more accessible for remote control (RC) pilots.

Many research groups are now working on quadrotors as UAV testbeds for control algorithms for autonomous control and sensing,[7,9-15] consistently selecting vehicle sizes in the range of 0.3 - 4.0 kg. Several testbeds have achieved control with external tethers and stabilizing devices. One such system,[7] based on the HMX-4, was flown, with the gyro augmentation system included with the vehicle active, and with X-Y motion constraints. Altitude and yaw control were demonstrated using feedback linearized attitude control. Backstepping control was applied for position, while state estimation was accomplished with an offboard computer vision system. Another tethered testbed[14] used an extensive outward facing sensor suite of IR and ultrasonic rangers to perform collision avoidance. Control of the vehicle was achieved using a robust internal-loop compensator, and computer vision was used for positioning. A third project[16] relied on a tether to use a POLYHEMUS magnetic positioning system. Tight position control at slow speeds was demonstrated using a nonlinear control technique based on nested saturation for lateral control with linearized equations of motion, and compensating in altitude control for the tilt of thrust vectors.

Other projects have relied on various nonlinear control techniques to perform indoor flights at low velocities without a tether. One such project,[11] consisting of a modified Draganflyer quadrotor helicopter, has demonstrated successful attitude and altitude control tests using a nonlinear control scheme. The OS4 quadrotor project[10] features its own vehicle design and identifies dynamics of the vehicle beyond the basic nonlinear equations of motion, including gyroscopic torque, angular acceleration of blades, drag force on the vehicle, and rotor blade flapping as being potentially significant, although the effects of the forces are not quantified or analyzed. A proportional-derivative (PD) control law led to adequate hovering capability, although the derivative of the command rate was not included in the control law to maneuver the vehicle. A Lyapunov proof proved stability of the simplified system in hover, and successful attitude and altitude control flights were achieved. A third project[12] achieved autonomous hover with IR range positioning to walls indoors, with a stability proof under the assumed dynamics. The system was modified to incorporate ultrasonic sensors,[17] and later incorporated two cameras for state estimation[18] as well.

Several vehicles saw success using Linear Quadratic Regulator (LQR) controllers on linearized dynamic models. The Cornell Autonomous Flying Vehicle (AFV)[13] was a custom airframe with brushless motors controlled by custom circuitry to improve resolution. Position control was accomplished using dead-reckoning estimation, with a human input to zero integration error. The MIT multi-vehicle quadrotor project[19] uses an offboard Vicon position system to achieve very accurate indoor flight of the Draganflyer V Ti Pro, and demonstrated multiple vehicles flying simultaneously. The vehicles are capable of tracking slow trajectories throughout an enclosed area that is visible to the Vicon system. It is possible to observe, in flight videos presented with the paper, the downwash from one vehicle disturbing another vehicle in flight, causing a small rocking motion, possibly due to blade flapping.

At Stanford, there has been prior work on quadrotor helicopters as well. First, the Mesicopter project[20] developed a series of small quadrotors, ranging from a few centimeters from motor to motor up to tens of centimeters. This work focused on rotor design, and also studied first order aerodynamic effects. Next came a separate project, the Stanford Testbed of Autonomous Rotorcraft for Multi-Agent Control (STARMAC). The first iteration was a testbed of two vehicles, STARMAC I aircraft, that performed GPS waypoint tracking using an inertial measurement unit (IMU), an ultrasonic ranger for altitude, and an L1 GPS receiver.[9] The testbed was derived from a Draganflyer aircraft, and weighed 0.7 kg. In order to improve attitude control, this project found that frame stiffening greatly improved attitude estimation from the IMU, leading to cross braces between the cantilevered motors. Also, aerodynamic disturbances in altitude were observed with this testbed, and modeled using flight data.[21]

Despite the substantial interest in quadrotor design for autonomous vehicle testbeds, little attention has been paid to the aerodynamic effects that result from multiple rotors, and from motion through the free stream. Exceptions to this trend, besides the Mesicopter project, include work from a group in Velizy, France[22] which investigates drag forces due to wind and presents a control law to handle such forces should they be estimated. Also, many important aerodynamic phenomenon were identified in the X-4 Flyer project

American Institute of Aeronautics and Astronautics

Figure 2. Thrust test stand used to measure thrust, side force, and torque using a load cell. Battery monitoring circuitry measures motor voltage and current. Data is captured to the computer using an Atmel microprocessor to measure the analog signal at 400 Hz.

at the Australian National University.[23] The project considers the effects of blade flapping, roll and pitch damping due to differing relative ascent rates of opposite rotors, as well as dynamic motor modeling. Preliminary results of the inclusion of aerodynamic phenomena in vehicle and rotor design show promise in flight tests, although an instability currently occurs as rotor speed increases, making untethered flight of the vehicle impossible.[15]

In the following sections, this paper extends the investigation of quadrotor aerodynamics, as they pertain to position control and trajectory tracking flight. The effects of aerodynamics on a moving quadrotor helicopter are analyzed, through theory, and by experiment. Results are given using the STARMAC II quadrotor helicopter, a new, higher thrust, reconfigurable vehicle. The next section presents the test apparatus used.

III.   Experimental Setup

The experimental equipment consisted of two primary components: a thrust test stand and prototype quadrotor aircraft, STARMAC II. The thrust test stand permitted research into the performance of individual motors and rotors, in varying flight conditions, while STARMAC II permitted experiments with an actual quadrotor vehicle through indoors and outdoors flight testing. This section presents the relevant details of the two systems.

A.   Thrust Test Stand

In order to evaluate motor and rotor characteristics, a thrust test stand was developed, shown in Figure 2. It measures the forces and torques using a load cell. The mounting point on the lever is adjustable to allow load sensitivity to be varied. An Atmel microprocessor board was programmed to perform motor control through its pulse width modulation (PWM) outputs, and to acquire analog inputs from the load cell, current sensor, and battery voltage.

The microprocessor board interfaces with a data acquisition program on the PC to perform automated tests, making measurements at 400 samples per second, well faster than the Nyquist frequency of the rotor rotation effects being measured. To perform some experiments, external wind was applied using a fan. Wind speeds were measured using a Kestral 1000 wind meter, with a rated accuracy of $\pm 3\%$.

B.   STARMAC II Quadrotor

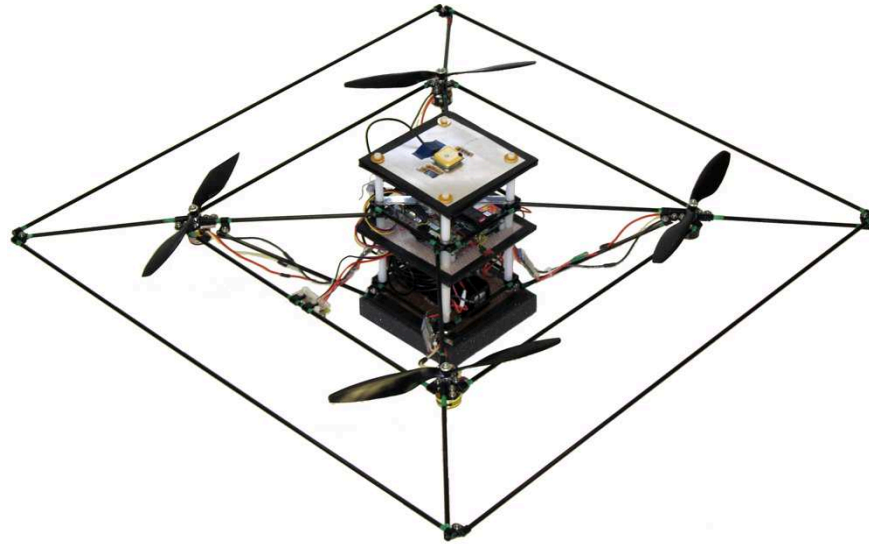The STARMAC vehicles were designed to meet five main requirements.

Figure 3. STARMAC II vehicle and its components.

1. Safe, simple operation both indoor and outdoor.

2. Autonomous position control and trajectory tracking.

3. Environmental perception through various sensors.

4. Communication with multiple vehicles and a ground station.

5. Onboard implementation of multi-vehicle coordination algorithms.

The first requirement drove the selection of the quadrotor vehicle as a safe, easy to use platform with very limited maintenance requirements. The ability to hover was deemed essential for operation in confined spaces, both indoor and outdoor. The second and third requirements drove the selection of the sensor suite to be included on board the vehicles, which in turn drove the payload requirements. The fourth requirement drove the need for a broadband communication device and the last requirement resulted in the inclusion of significant computational power. Ultimately, the key tradeoff was between keeping the vehicle small enough to be flown without too many special precautions for ensuring safety, and making it large enough to be able to support the necessary payload to achieve the tasks required for the many applications envisaged for it.

The vehicle frame, visible in Figure 3 was designed to be as light as possible, while maintaining sufficient stiffness to ensure accurate state measurement and control actuation. Constructed of carbon fiber tubes, honeycomb platforms, plastic fasteners and Delran motor mounts, the entire frame weighs approximately 150g, or less than 15% of the total mass of the vehicle in its lightest configuration. In order to minimize vibrational effects on inertial measurement and to ensure consistent thrust actuation, crossbraces were added which significantly improved vertical stiffness of the motor mount location, as well as torsional rigidity of the core. A protective outer bar was added to prevent rotor impingement in flight, and help make the vehicle safer to fly in close proximity to obstacles. The plastic fasteners allow the frame to be reconfigured to carry different payloads, and to perform aerodynamic experiments.

The thrust is provided by Axi 2208 brushless motors,[24] Wattage 10×4.5 Park Flyer props (both tractor and pusher),[25] and Castle Creations Phoenix 25 speed controllers,[26] resulting in up to 8 N of thrust per motor for a total max gross thrust of 32 N. The vehicle can operate at up to 2.5 kg total mass, limited by steady state current constraints of the small motors. Thrust margin for control is also required, though this is not an active constraint due to the steady state current limitations. The brushless motors also allow

American Institute of Aeronautics and Astronautics

for direct drive of the rotor without significant efficiency loss, thereby eliminating the need for gearing, one cause of vibration in earlier designs.

The vehicle is equipped with three separate sensors for full state estimation. A Microstrain 3DMG-X1 IMU[27] provides three-axis attitude, attitude rate and acceleration, through a built-in estimation algorithm which relies on three gyroscopes, three accelerometers and three magnetometers. The resulting attitude estimates are accurate to $\pm 2°$, so long as sustained accelerations are not maintained. Height above the ground is determined using a sonic ranging sensor, either the Devantech SRF08 (2 m range, in practice, 0.018 kg[28]) or the Senscomp Mini-AE (9 m range, 0.035 kg[29]). With a relatively wide ranging cone of $20°$, these sensors effectively measure the shortest path to the ground with 3-5 cm accuracy, despite non-zero pitch and roll angles in flight. Three-dimensional position and velocity measurements are made using carrier phase differential GPS relying on the Novatel Superstar II GPS unit,[30] for which a custom code was developed in house to keep both weight and cost down. The unit outputs raw integrated carrier phase measurements at 10 Hz and the resulting position accuracy is 1-2cm relative to a stationary base station. An onboard Extended Kalman Filter is used to combine GPS and raw inertial measurements for accurate full state estimation. For indoor flights, an overhead USB camera is used, with blob tracking software, to provide position sensing in place of GPS. The camera system gives 1-2 cm accuracy at a rate of 10 Hz, and provides a drop-in replacement for GPS input to the Kalman Filter.

Computation and control are managed at two separate levels. The low level control, which performs real-time control loop execution and outputs PWM motor commands, occurs on a Robostix microcontroller board[31] based on the Atmega 128 processor. The high level planning, estimation and control occurs on either a lightweight Crossbow Stargate 1.0 single board computer (SBC)[32] running embedded Linux on a PXA255 microprocessor, or on an Advanced Digital Logic ADL855 PC104+[33] running Kubuntu Linux. The Stargate SBC (0.05 kg) provides sufficient computational resources for carrier phase differential GPS calculations and can be used to perform autonomous position control without the ability to add additional coordination algorithms between vehicles. As an alternative, the PC104 (0.48 kg) provides a wealth of computation power, at the cost of additional weight and hence, shortened flight times. Communications for the high level computers are managed through UDP over a WiFi network. The Stargate uses 802.11b, and the ADL855 uses 802.11g.

The baseline configuration results in a takeoff weight of 1.1 kg with the Stargate SBC, and 1.6 kg with the PC104. Using one 4200 mAH Lithium Polymer battery from ThunderPower,[34] vehicle flight times fall in the range of 15-20 minutes, though more batteries could be flown to extend flight time. A custom printed circuit board distributes power and provides necessary communications interfaces. Using this board, battery replacement can be performed without power interruption.

The vehicle is able to carry additional payload, up to the 2.5 kg limit, allowing it to be reconfigured for specific applications. Numerous additional sensors have been tested on the STARMAC platform, including the Videre Systems stereo vision camera,[35] the Hokuyo-URG laser range finder[36] and the Tracker DTS digital avalanche beacon and receiver.[37] The system is designed to function as an independent sensing and computing platform, to enable the vehicles to perform multi-agent missions, such as cooperative search and rescue.[1]

IV. Vehicle Dynamics

The derivation of the nonlinear dynamics is performed in North-East-Down (NED) inertial and body fixed coordinates. Let $\{\mathbf{e_N}, \mathbf{e_E}, \mathbf{e_D}\}$ denote unit vectors along the respective inertial axes, and $\{\mathbf{x_B}, \mathbf{y_B}, \mathbf{z_B}\}$ denote unit vectors along the respective body axes, as defined in Figure 4. Euler angles of the body axes are $\{\phi, \theta, \psi\}$ with respect to the $\mathbf{e_N}$, $\mathbf{e_E}$ and $\mathbf{e_D}$ axes, respectively, and are referred to as roll, pitch and yaw. The current velocity direction unit vector is $\mathbf{e_v}$, in inertial coordinates, and defines coordinates relative to the c.g. referred to as longitudinal, lateral and vertical. The rotor plane does not necessarily align with the $\mathbf{x_B}$, $\mathbf{y_B}$ plane, so for the ith rotor let $\{\mathbf{x_{R,i}}, \mathbf{y_{R,i}}, \mathbf{z_{R,i}}\}$ denote unit vectors aligned with the plane of the rotor and oriented with respect to the lateral, longitudinal, and vertical directions as shown in Figure 5. Let $\mathbf{r}$ be defined as the position vector from the inertial origin to the vehicle center of gravity (c.g.), and let $\omega_\mathbf{B}$ be defined as the angular velocity of the aircraft in the body frame.
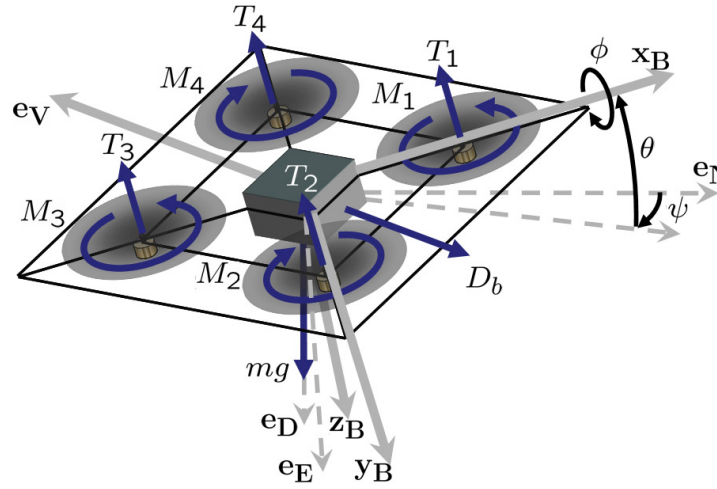
American Institute of Aeronautics and Astronautics

Figure 4. Free body diagram of a quadrotor helicopter. The roll, pitch and yaw angles (ϕ, θ, and ψ, respectively) are controlled by differential thrust. Differential thrust between opposite motors provides roll and pitch torques. Differential thrust between the two pairs of counter-rotating motors provides yaw torque. Position control, with respect to the North-East-Down (NED) coordinate frame is accomplished by controlling the magnitude and direction of the total thrust. A drag force, D_b, also acts on the vehicle, opposite the velocity direction, $\mathbf{e_V}$.

The rotors, numbered $1 - 4$, are mounted outboard on the $\mathbf{x_B}$, $\mathbf{y_B}$, $-\mathbf{x_B}$ and $-\mathbf{y_B}$ axes, respectively, with position vectors $\mathbf{r}_i$ with respect to the c.g. Thrust is produced by each rotor through the torque applied by brushless DC motors, with the dynamics of each motor given by

$$Q = K_q I \tag{1}$$
$$V = R_a I + K_e \omega \tag{2}$$

where Q is the torque developed by the motor, V is the voltage across the motor, I is the current through the motor, and ω is the angular rate at which the motor is spinning.[38] K_q, R_a, and K_e are motor-specific constants, where K_q relates current to torque, R_a is the total armature resistance of the motor, and K_e relates motor speed to the back EMF. Converting voltage to power in steady state gives

$$P = IV = \frac{Q}{K_q} V \tag{3}$$

which can be related to thrust by equating the power produced by the motors to the ideal power required to generate thrust by increasing the momentum of a column of air. The ideal power is the thrust force times the speed it is applied at. At hover, this power, P_h, is

$$P_h = T v_h \tag{4}$$

where the induced velocity at hover, v_h, is the change in air speed induced by the rotor blades with respect to the free stream velocity, v_∞. For this analysis, the free stream velocity is set to be zero, for wind-free hover conditions. For general flight, the induced velocity is denoted v_i, as used in later sections. Using momentum theory,[4]

$$v_h = \sqrt{\frac{T}{2\rho A}} \tag{5}$$

where T is the thrust produced by the rotor to remain in hover, $A = \pi R^2$ is the area swept out by the rotor, ρ is the density of air and R is the radius of the rotor. For a quadrotor helicopter, this is equal to

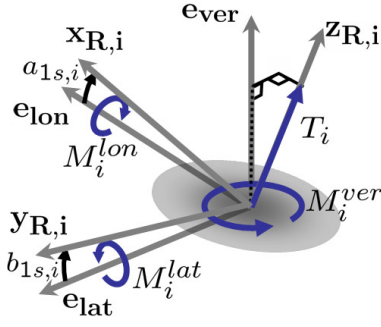American Institute of Aeronautics and Astronautics

Figure 5. Free body diagram of the moments and forces acting on rotor i. Due to the effect of "blade flapping", explained in Section V, the thrust and moments that were depicted in Figure 4 are not necessarily orthogonal to the body axes. They undergo deflection depending on the velocity of the vehicle and the direction of spin of the specific rotor. The unit vector $\mathbf{e_{ver}}$ is parallel to the body vertical direction, $\mathbf{z_B}$, $\mathbf{e_{lon}}$ is parallel to the velocity vector, $\mathbf{e_v}$, and $\mathbf{e_{lat}}$ is orthogonal to both. The thrust is deflected by small angles $a_{1s,i}$ and $b_{1s,i}$. This deflection also results in reaction moments about the rotor hub.

$\frac{1}{4}T_{nom}$, where the nominal weight T_{nom} is equal to the weight of the vehicle. The torque is proportional to the thrust,[4] with a constant ratio κ_t that depends on blade geometry. The relation between applied voltage and thrust is found by equating the power produced with the ideal power consumed at hover, and combining equations (4) and (5), to yield

$$\frac{Q}{K_q}V = \frac{\kappa_t T}{K_q}V = \frac{T^{3/2}}{\sqrt{2\rho A}} \tag{6}$$

Thus,

$$T = \frac{2\rho A \kappa_t^2}{K_q^2}V^2 \tag{7}$$

The thrust produced by the rotors is proportional to the square of the voltage across the motor. Each of the four rotors produces a thrust, denoted T_i, controlled through the application of a voltage V_i, which is used to actuate the vehicle.

The thrust produced by the ith rotor acts perpendicularly to the rotor plane along the $\mathbf{z_{R,i}}$ axis, as defined in Figure 5. Each rotor also produces an aerodynamic moment, $\mathbf{M}_i$, in the body fixed frame, which is a function of the motor torque as well as various aerodynamic effects which are described in Section V. The roll, pitch and yaw angles are controlled by differential thrust. Differential thrust between opposite motors provides roll and pitch torques. Differential thrust between the two pairs of counter-rotating motors provides yaw torque. To decouple the control, motors 1 and 3 rotate in the opposite direction of rotors 2 and 4.

The vehicle body drag force is defined as D_b, vehicle mass is m, acceleration due to gravity is g, and the inertia matrix is $I_b \in \mathbb{R}^{3\times3}$. A free body diagram is depicted in Figure 4, with a depiction of the rotor forces and moments in Figure 5. The total force, $\mathbf{F}$, can be summed as,

$$\mathbf{F} = -D_b\mathbf{e_v} + mg\mathbf{e_D} + \sum_{i=1}^{4}\left(-T_i R_{R_i,I_b}\mathbf{z_{R,i}}\right) \tag{8}$$

where $R_{R_i,I}$ is the rotation matrix from the plane of rotor i to inertial coordinates[a]. Similarly, the total moment, $\mathbf{M}$, is,

$$\mathbf{M} = \sum_{i=1}^{4}\left(\mathbf{M}_i + \mathbf{r_i} \times \left(-T_i R_{R_i,B}\mathbf{z_{R,i}}\right)\right) \tag{9}$$

---

[a]The notation $R_{A,B}$ shall refer to rotation matrices from coordinate system A to B throughout.

where $R_{R_i,B}$ is the rotation matrix from the plane of rotor i to body coordinates. Note that the drag force was neglected in computing the moment. This force was found to cause a negligible disturbance on the total moment over the flight regime of interest, relative to blade flapping torques. The full nonlinear dynamics can be described as,

$$\mathbf{F} = m\ddot{\mathbf{r}} \tag{10}$$

$$\mathbf{M} = I_b\dot{\omega}_{\mathbf{B}} + \omega_{\mathbf{B}} \times I\omega_{\mathbf{B}} \tag{11}$$

where the total angular momentum of the rotors is assumed to be near zero, as the momentum from the counter-rotating pairs cancels when yaw is held steady.

V.   Aerodynamic Effects

Although quadrotor vehicle dynamics are often assumed to be accurately modeled as linear for attitude and altitude control, this assumption is only reasonable at slow velocities. Even at moderate velocities, the impact of the aerodynamic effects resulting from variation in air speed is significant. This section focuses on four main effects, three of which are quantifiable and are incorporated into the nonlinear dynamics model of the vehicle for estimation and control, and one which results in unsteady airflow and can therefore be mitigated through structural redesign.

The three quantifiable aerodynamic effects relate to motion of the vehicle relative to the free stream. The first effect is that the total thrust varies not only with the power input, but with the free stream velocity, and the angle of attack with respect to the free stream. This is further complicated by a flight regime, called vortex ring state, in which there is no analytical solution for thrust, and experimental data shows that the thrust is extremely stochastic. The second effect results from differing inflow velocities experienced by the advancing and retreating blades. This leads to "blade flapping" which induces roll and pitch moments on the rotor hub as well as a deflection of the thrust vector. The third effect is the interference caused by the vehicle body in the slip stream of the rotor. It results in unsteady thrust behavior, rendering attitude tracking difficult. This effect was demonstrated to be significantly reduced by airframe modifications.

A.   Total Thrust

The induced power is the required power input to create the induced velocity. As a rotorcraft undergoes translational motion, or changes angle of attack, the induced power requirement of a rotorcraft changes. Note that v_{∞} is the total free stream speed, including translational velocity and ambient wind velocity. To derive the effect of free stream velocity on induced power, from conservation of momentum, the induced velocity, v_i for an ideal vehicle can be found by solving[4]

$$v_i = \frac{v_h^2}{\sqrt{(v_{\infty}\cos\alpha)^2 + (v_{\infty}\sin\alpha + v_i)^2}} \tag{12}$$

for v_i, where α is the angle of attack, with positive corresponding to pitching forward. The solution to this equation has reduced accuracy for large angles of attack, and is not valid during vortex ring state, as will be described below. Nonetheless, it provides an accurate result for much of the useful flight envelope. Experimental results showing the accuracy of this equation as a function of flight envelope have been established in the literature.[39] The analytical solution for v_i is the solution to the quartic polynomial of equation (12), and its expression is too large to include, though it can be easily computed numerically. Using the expression for v_i, or a numerical solution, the ideal thrust per power input can be computed, using

$$T = \frac{P}{v_{\infty}\sin\alpha + v_i} \tag{13}$$

where the denominator corresponds to the air speed across the rotors.

The value of the ratio of thrust to hover thrust, T/T_h, is plotted for the v_h of STARMAC II, in Figure 13. At low speeds, the angle of attack has vanishingly little effect on T/T_h. However, as speed increases, the
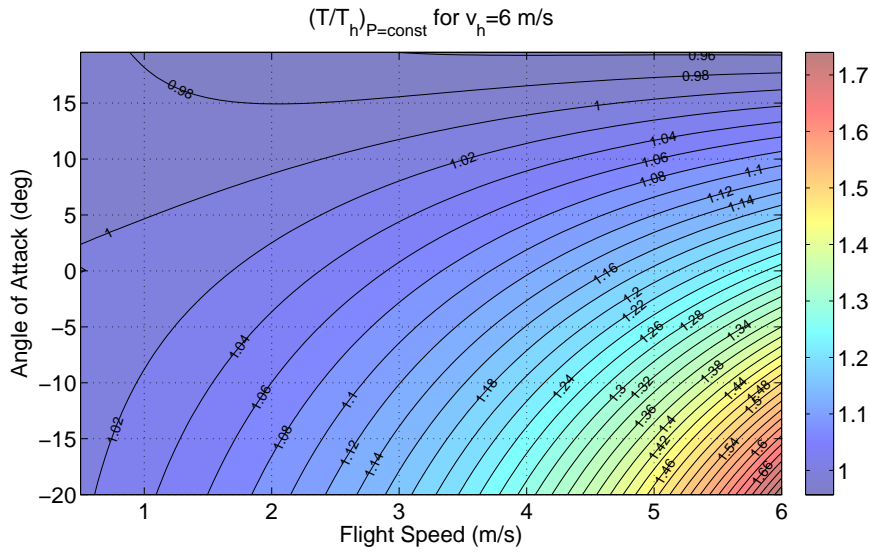
Figure 6. The thrust generated at a constant power, P_{const}, varies depending on vehicle's speed and angle of attack relative to the incoming flow (the angle of attack is positive when pitching down). As speed increases, the variation of thrust with the angle of attack becomes more extreme, causing strong control disturbances, particularly in attitude, as shown in Figure **13**. At high speeds, the flight dynamics resemble those of an airplane.

ratio T/T_h becomes increasingly sensitive to the angle of attack, varying by a substantial fraction of the aircraft's capabilities, within the flight envelope. Similar to an airplane, pitching up increases the lift force. The angle of attack for which thrust is at the hover value increases with forward speed. For level flight, the power required to retain altitude increases with the forward speed.

In the extreme regions of angle of attack, where flight is close to vertical, rotorcraft have three operational modes for climb velocity,[4] v_c, two of which can be understood as simplifications of the above quartic equation (where $\cos \alpha = 0$), and one of which is a recirculation effect that significantly reduces rotor efficiency. Note that this flight regime would be normal for a vertical ascent or descent. The three modes are defined as follows:

1. Normal working state: $0 \leq \frac{v_c}{v_h}$

2. Vortex ring state (VRS): $-2 \leq \frac{v_c}{v_h} < 0$

3. Windmill brake state: $\frac{v_c}{v_h} < -2$

In normal working state, air is flowing down through the rotor. In windmill brake state, air is flowing up through the rotor due to rapid descent. For these two states, conservation of momentum can be used to derive the induced velocity. For the normal working state, the hover and ascent condition, the induced velocity is[4]

$$v_i = -\frac{v_c}{2} + \sqrt{\left(\frac{v_c}{2}\right)^2 + v_h^2} \tag{14}$$

For the windmill braking state, rapid descent, the induced velocity is,

$$v_i = -\frac{v_c}{2} - \sqrt{\left(\frac{v_c}{2}\right)^2 - v_h^2} \tag{15}$$

In the vortex ring state, air recirculates through the blades in a periodic and somewhat random fashion. As a result, the induced velocity varies greatly, particularly over the domain $-1.4 \geq v_c/v_h \geq -0.4$, reducing

American Institute of Aeronautics and Astronautics

aerodynamic damping.[39] An empirical model[4] of induced velocity in vortex ring state is

$$v_i = -v_h \left(\kappa + k_1 \left(\frac{v_c}{v_h} \right) + k_1 \left(\frac{v_c}{v_h} \right) + k_2 \left(\frac{v_c}{v_h} \right)^2 + k_3 \left(\frac{v_c}{v_h} \right)^3 + k_4 \left(\frac{v_c}{v_h} \right)^4 \right) \tag{16}$$

where $k_1 = -1.125$, $k_2 = -1.372$, $k_3 = -1.718$, $k_4 = -0.655$. This model compares with the mean of experimental results in the literature, though it fails to capture the periodic nature of the vortex entrapment.

To model the dynamics during climb, the power is the thrust times the speed it is applied at,

$$T = \frac{P}{v_c + v_i} \tag{17}$$

ignoring profile power losses. Note that Tv_c is the power consumed by the climbing motion, whereas Tv_i is the power transferred into the air. It is typically desirable to avoid the vortex ring state, which can be done by maintaining a substantial forward speed while descending.[3]
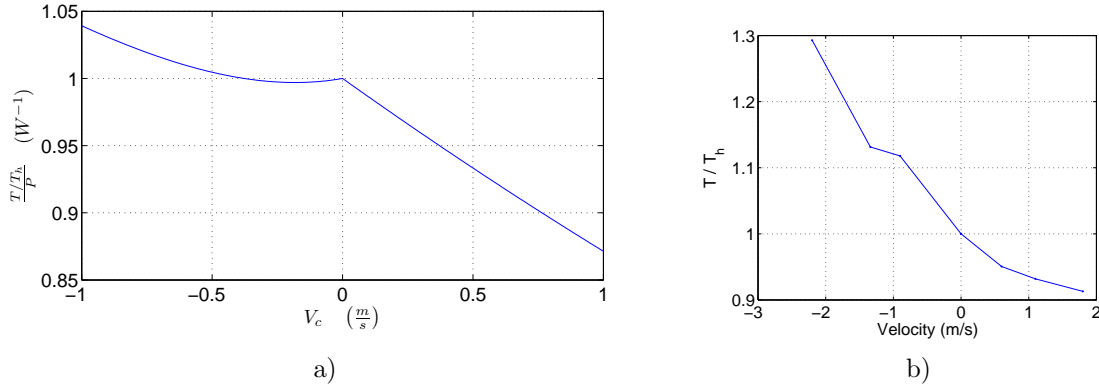

a)   b)

Figure 7. a) Theoretically predicted effect of climb velocity, v_c, on normalized thrust, per unit of power input. b) Thrust test stand measured effect of v_c on normalized thrust. The hover velocity is for a vehicle with the same parameters as STARMAC II. In ascent, there is a virtual damping force close to linearly proportional to speed. However, for descent at a slow velocity, there is no damping force, rather there may be a small negative damping force. The ascent equations are based on momentum conservation of the airstream, and the descent equations are based on published experimental curve fits.

The thrust achieved for a given input power can be computed as a function of climb velocity by substituting equation (14), equation (15), and equation (16) into equation (17). For the flight conditions experienced by STARMAC II, the ratio of the thrust to hover thrust, per power input, is shown in Figure 7, where plot a) is the theoretical curve, using the solution to the above equations, and plot b) shows data from a thrust test stand experiment using a vertical wind disturbance. As is visible in Figure 7-a), there is a clear loss of thrust associated with climbing, reducing linearly with climb velocity. The vortex ring state has an essentially negligible impact on thrust relative to hover thrust, although in practice, this recirculating flow regime is much more variable, and hence undesirable. Finally, a significant negative climb velocity results in an increase in resulting thrust.

In thrust test stand experiments, the loss of thrust with an applied climb velocity was clearly noted. The descent velocity experiments were much less conclusive. For low speeds, there is little evidence of the vortex ring state losses, suggesting that the establishment of a vortex ring was not achieved with the test stand apparatus. It must be noted that increased vibration was observed, however, which indicates that unsteady flow did occur. The average thrust remained close to the zero climb velocity value, though it oscillated substantially, making assessment of the change in thrust difficult.

B. Blade Flapping

The second aerodynamic effect to have a significant effect on the dynamics of quadrotor vehicles is blade flapping. In translational flight, the advancing blade of a rotor sees a higher effective velocity relative to the
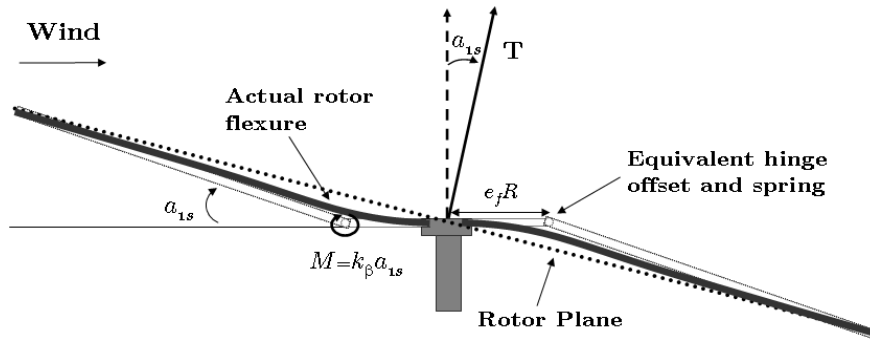
Figure 8. Diagram representing the effects of rotor blade flapping[5] and the modeling of stiff rotor blades as hinged blades with an effective offset and blade stiffness k_β.[3] The rotor plane becomes tilted, resulting in a deflection of the thrust vector, and a moment is generated at the blade root.

air, while the retreating blade sees a lower effective velocity. This results in a difference in lift between the two rotors, causing the rotor blades to flap up and down once per revolution.[5] This flapping of the blades tilts the rotor plane back away from the direction of motion, which has a variety of effects on the dynamics of the vehicle, in particular affecting stability in attitude.[15] For this subsection, the effects on an individual rotor will be considered, so for readability, the rotor index, subscript i, is implied but not written. The backwards tilt of the rotor plane generates a longitudinal thrust, T_{lon},

$$T_{b,lon} = T \sin a_{1s} \tag{18}$$

where a_{1s} is the angle by which the thrust vector T is deflected (see Figure 8). If the center of gravity of the vehicle is not aligned with the rotor plane, this longitudinal force will generate a moment about the c.g., $M_{b,lon} = T_{b,lon} r_{cg}$, where r_{cg} is the vertical distance from the rotor plane to the c.g. of the vehicle. For stiff rotors, as are used in most current quadrotor helicopters, the tilt of the blades also generates a moment at the rotor hub

$$M_{bs} = k_\beta a_{1s} \tag{19}$$

where k_β is the stiffness of the rotor blade in Nm/rad.

Coning (the upward flexure of the rotor blades from the lift force on each blade) also causes the impinging airflow to have unbalanced forcing of the blades which causes a lateral tilt of the rotor plane, the details of which are developed in the literature.[5] This lateral tilt generates moments at right angles to the velocity vector, but because of the counter-rotating pairs of quadrotor rotors, the lateral effects cancel. For stiff 2-bladed rotors, the moments due to the coning angles are symmetric about the rotor hub and also cancel.

A distinction must be noted here in the use of the terminology flap angle β and deflection angle a_{1s}. The flap angle β of a rotor blade is typically defined in the helicopter literature as the total deflection of a rotor blade away from the horizontal in body coordinates at any point in the rotation, and is calculated as

$$\beta = a_{0s} - a_{1s} \cos \Psi + b_{1s} \sin \Psi \tag{20}$$

where a_{0s} is the blade deflection due to coning, a_{1s} and b_{1s} are the longitudinal and lateral blade deflection amplitudes, respectively, due to flapping. Ψ is the azimuth angle of the blade, and is defined as zero at the rear. Since coning affects both blades equally, the deflection of the thrust vector is due to both longitudinal and lateral tilts. For quadrotor vehicles, however, the moments generated by lateral deflections cancel, and generation of unbalanced moments is due entirely to the longitudinal deflection, a_{1s}. The longitudinal deflection gives the amplitude of the rotor tilt fore and aft ($\Psi = \pi$, 0 rad), which we will refer to from here on as the deflection angle to avoid confusion with the flapping angle, β.

The equation for deflection angle of a flapping rotor with hinged blades is[15]

$$a_{1s} = \frac{1}{1 + \frac{\mu_{lon}^2}{2}} \frac{4}{3} \left(\frac{C_T}{\sigma} \frac{2}{3} \frac{\mu_{lon}\gamma}{a_0} + \mu_{lon} \right) \tag{21}$$

where a_0 is the slope of the lift curve per radian (typically about 6.0 for conventional airfoils at low Mach numbers according to literature[5]), μ_{lon} is the longitudinal rotor advance ratio, defined as the ratio of the longitudinal to blade tip speed,

$$\mu_{lon} = \frac{v_{lon}}{v_t} \tag{22}$$

and γ is the nondimensional Lock number, which gives the ratio of aerodynamic to centrifugal forces and is defined as

$$\gamma = \frac{\rho a_0 c R^4}{I_b} \tag{23}$$

where I_b is the moment of inertia of the blade about the hinge, c is the chord of the blade, and R is the rotor radius. σ is the solidity ratio of the rotor, and is defined as

$$\sigma = \frac{A_b}{A} \tag{24}$$

where A_b is the total area of the rotor blades.

Equation (21) predicts a roughly linear relationship between velocity and deflection angle in the STAR-MAC II operating regime. In practice, this equation over-predicts the flapping seen by rotors with unhinged blades (see Figure 9) where the stiffness of the blades must be accounted for.

The flapping properties of a stiff, fixed-pitch rotor blade can be analyzed by modeling the blade as being hinged at an effective offset e_f from the center of rotation (expressed as a percentage of the rotor radius) and a torsional spring with stiffness k_β Nm/rad at the hinge .[3] This approximates the first bending mode of the blade and is sufficient for the small angles we are concerned with. Both e_f and and k_β can be determined by measuring the natural frequency ω_n of blade vibration and using the following relations:[3,5]

$$\omega_n = \sqrt{\frac{k_\beta}{I_b}} \tag{25}$$

$$e_f = \frac{1}{\frac{3}{4}\frac{b\Omega^2 I_b}{k_\beta}} \tag{26}$$

where b is the number of blades and I_b is the moment of effective moment of inertia of the blade about the hinge at e_f. Substituting equation (25) into equation (26), we have

$$e_f = \frac{1}{\frac{3}{4}\frac{b\Omega^2}{\omega_n^2}} \tag{27}$$

The constants k_β and I_b can be obtained by determining the force required at the tip to deflect the blade through some angle δ and balancing moments:

$$F(1 - e_f)R\delta = k_\beta \delta \tag{28}$$

Substituting the value for k_β determined in equation (28) back into equation (25) yields I_b. With these parameters, the equilibrium flapping constants can be determined by solving[3]

$$
\begin{bmatrix}
\lambda_\beta^2 & 0 & 0 & 0 \\
\frac{\gamma}{6}\mu_{lon} & (1 - \lambda_\beta^2) & -\frac{\gamma}{8} & 0 \\
0 & \frac{\gamma}{8} & (1 - \lambda_\beta^2) & 0 \\
0 & 0 & 0 & 1
\end{bmatrix}
\begin{bmatrix}
a_{0s} \\
a_{1s} \\
b_{1s} \\
\frac{C_T}{\sigma a_0}
\end{bmatrix}
=
\begin{bmatrix}
\frac{\gamma}{8} & -\frac{\gamma}{6} \\
0 & 0 \\
\frac{\gamma}{3}\mu_{lon} & 0 \\
\frac{1}{3} & -\frac{1}{2}
\end{bmatrix}
\begin{bmatrix}
\Theta_{avg} \\
\mu_{ver} + \lambda_i
\end{bmatrix}
\tag{29}
$$

Equation (29) depends heavily on several parameters. Once again, μ_{lon} and μ_{ver} are the horizontal and vertical advance ratios, respectively ($\mu_{ver} = 0$ in translational flight). Θ_{avg} is the average pitch angle of the blade. λ_β is the ratio of the flapping frequency ω_β to the angular rate Ω of the rotor, and for stiff propellers is defined as

$$\lambda_\beta = \frac{\omega_\beta}{\Omega} \tag{30}$$
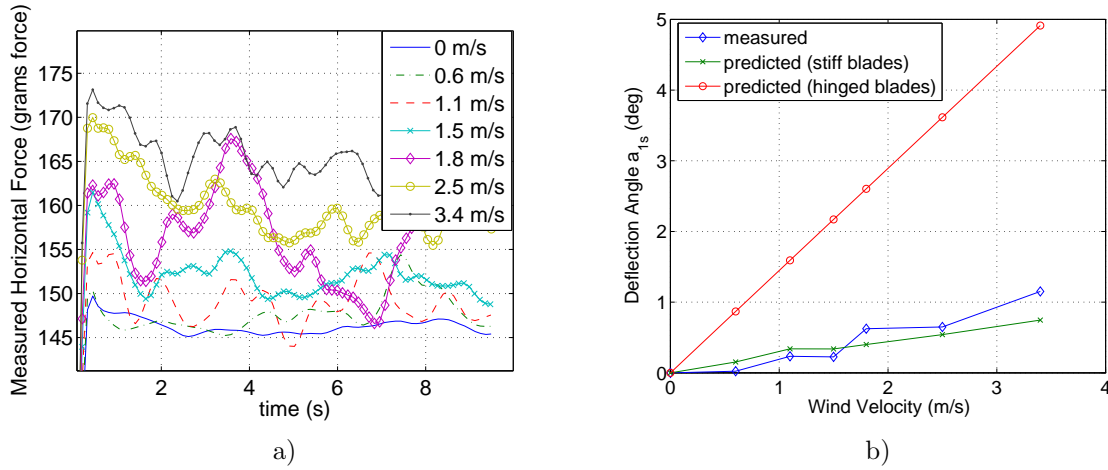
American Institute of Aeronautics and Astronautics

Figure 9. a) Horizontal force is measured at different wind velocities in order to calculate the flapping angles and to see the effect of flapping. b) The measured deflection angle is compared with predicted values using equations which assume hinged, freely flapping blades and more complex ones which model stiff, unhinged blades. The hinged equations greatly over-predict the flapping effect if used to analyze the behavior of stiff blades.

and can be calculated for use in equation (29) as

$$\lambda_\beta = \sqrt{(1 + \frac{3}{2}e_f) + \frac{k_\beta}{I_b\Omega^2}} \tag{31}$$

The lateral force due to the deflection of the thrust vector by flapping was measured for a single rotor by blowing air at fixed velocities across a spinning rotor attached to the test stand. This data was filtered and used to calculate the average deflection angle as a function of incident wind velocity and compared to the predictions of the flapping equations from literature.[3] ω_β for the flapping equations was also measured using the test stand, giving an effective hinge offset of 25%. The value for k_β was measured to be $0.23Nm/rad$. The results are plotted in Figure 9. It should be noted that turbulence in the incident airflow caused oscillations in the blade deflection during experiments, so the measurements presented are an average deflection over a period of 20s.

C. Airflow Disruption

The STARMAC II airframe design underwent several iterations, thanks to the easily reconfigured plastic joints. The initial airframe used protective shrouds, had the rotors closer to the center, and had structural obstructions directly beneath the rotors. It was found that vortex impingement on the airframe had a significant effect on attitude stability. The stochastic nature of the forces of the vortices rendered vehicle control by differentially controlled thrust difficult.

Yaw control is achieved by giving differential commands to rotors spinning in opposite directions to generate a torque about the vertical axis which is used for control through a PID controller. The torque of a motor at a given command voltage depends on the airflow through the rotor. It was found that with protective shrouds in place, with a gap from the rotor of 5% a rotor radius, that it was very difficult to obtain consistent yaw tracking performance (see Figure 10 a). The shrouds were simple protective enclosures which were not designed with aerodynamic considerations. With the shrouds removed, yaw tracking instantly improved from errors of roughly $\pm 10°$ to less about $\pm 3°$ (see Figure 10 b). Subsequent analysis of the data showed that during shrouded flights, measured angular accelerations of the vehicle did not consistently match with motor commands. The most likely explanation is that the shrouds were disturbing or disrupting the flow of air through the rotors, causing the actual motor torque to vary for a given commanded voltage level. Replacing the shrouds with fixed guards away from the rotors eliminated this problem.
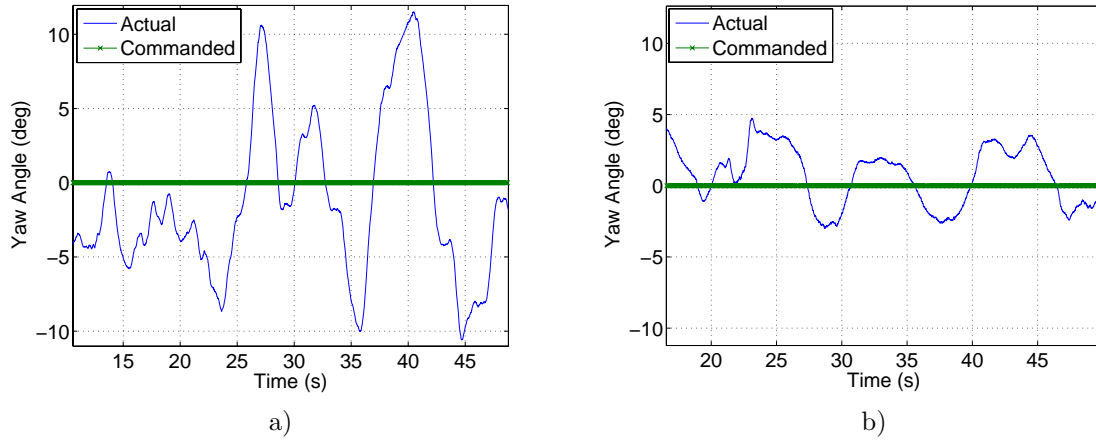
American Institute of Aeronautics and Astronautics

Figure 10. The effect of shrouds on yaw control. a) With shrouds, unless the shrouds are built to very exacting specifications, yaw control performance is highly variable since instability in the air flowing through the shrouds leads to highly varying torques on the rotors. b) With the shrouds removed, performance of the yaw control loop is instantly improved.

Similarly, pitch and roll control are achieved by giving differential commands to rotors on opposite sides of the aircraft. When the rotors were mounted close to the center of the vehicle, substantial attitude noise was introduced. It was found through experiment that this attitude noise was partially mitigated when the rotors were moved far enough from the core that the tip vortices no longer seemed to impinge on the structures at the core of the vehicle. In order to further reduce the noise, the position of the core brace mounts connecting the main carbon fiber tubes was varied. They were initially located at half a blade radius from the motor. Moving the mount toward the blade tip verified the hypothesis that proximity of any component of structure to the blade tip vortices could yield strong random disturbances. Indeed, the aircraft was not flyable with the mount near the blade tip. Upon moving the mount to coincide with the center of the motor, this random disturbance was eliminated.

The aircraft configuration depicted in Figure 1 is capable of accurately tracking control inputs, free of a substantial fraction of the possible random disturbances due to slip stream interaction with the frame.

VI.   Flight Results

This section presents flight tests results for attitude, altitude and position control on the STARMAC quadrotor vehicle. The control laws used for these flight tests treat the aerodynamics presented above as disturbances, although by using techniques such as accelerometer feedback, the achieved thrust can be more directly controlled to the desired value. Extension of the control design to feed forward the full suite of identified aerodynamic effects remains a task for future work.

A.   Attitude Flight Control

At low velocities and with small aerodynamic disturbances (for example in indoor flight), proportional-integral-derivative (PID) control is fully sufficient for good tracking of commanded attitude since the vehicle approximates a double-integrator with a first-order lag from the motor dynamics. For initial test flights indoors with STARMAC, good tracking was obtained even without an integrator for pitch and roll (see Figure 11) giving tracking errors on the order of $2 - 3°$.

In translational flight, the pitch and roll dynamics of a quadrotor are very sensitive to rotor blade flapping. In Figure 12, the effects of the blade flapping moments and c.g. location can be seen during a step input in the pitch command. Initially, the control effort commanded by the PD controller is sufficient to bring the vehicle toward the commanded pitch. As the speed increases, the restoring moments caused by blade
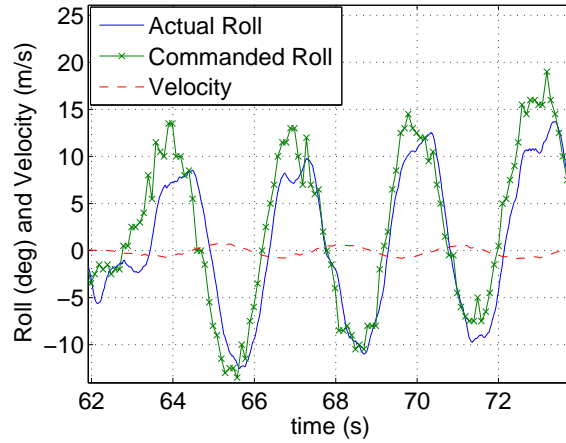
Figure 11. At low velocities, i.e. for small displacements from hover, a PID controller is sufficient for good attitude control.

flapping increase until the commanded torque is insufficient to hold the vehicle at commanded pitch despite an increase in the pitch error. It is possible to apply integral control to account for this effect to some extent, although it is important to understand that the integrator accounts for constant biases most effectively, and so eventually compensates for the pitch moment caused by a specific velocity only if the velocity is held constant. The integrator, therefore, will need to adapt each time the vehicle speeds up or slows down.

B.   Altitude Flight Control

Altitude control is provided by a linear controller with gain on the vertical acceleration as well as the usual PID terms. In general, the controller has proved to be very effective in altitude control, though performance can be improved by better filtering of the ultrasonic altitude sensor readings (see Figure 13a). It must provide strong active damping whenever descent velocity is encountered. Otherwise, altitude oscillations have been
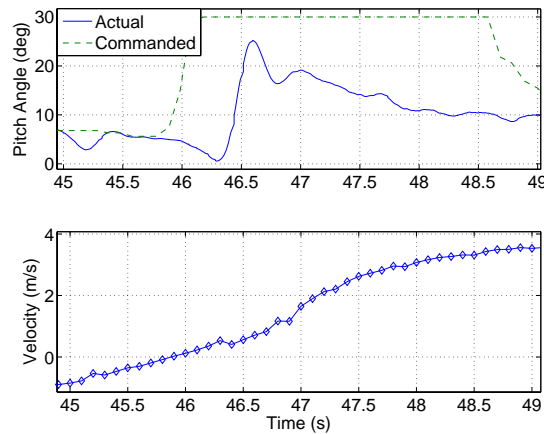

Figure 12.   The effect of rotor blade flapping is shown in the vehicle's response to a step input command in pitch angle. The quadrotor's control system uses proportional and derivative feedback only, so that the tracking error is proportional to the disturbance torque applied. As the aircraft translates, the thrust vector is deflected, causes a restoring moment about the c.g., adding to the moment from the flapping of the blades to force the vehicle to tilt back.
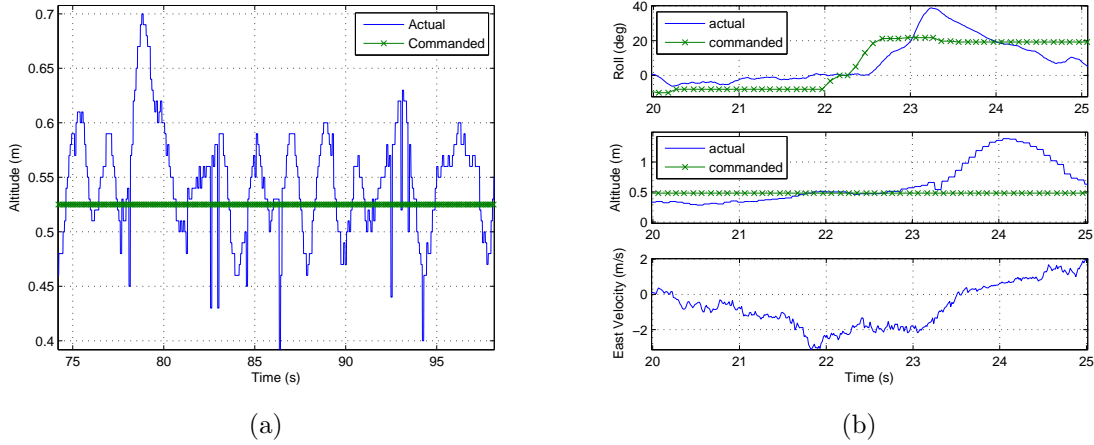
Figure 13. The effect of angle of attack and velocity on thrust is demonstrated during a flight with human-commanded attitude. (a) Altitude data from a typical flight near hover with sinusoidal roll commands, with a usual error of ±10 cm or less. The sharp spikes are noise in the ultrasonic altitude sensor. (b) Data from a subsequent flight. At just past 22 s, a positive roll is commanded to reduce the vehicle's westward velocity (the vehicle is aligned such that the roll axis points north/south). As the vehicle rolls through $0°$, it still has a large non-zero velocity, giving it zero angle of attack relative to the incoming flow. This causes the thrust for the currently applied power to rapidly increase (see Figure 6), causing a disturbance that pushes the vehicle above the commanded altitude.

observed to occur, due to an apparent drop in thrust during small descent velocities, as predicted by the induced velocity model results. However, with strong damping, this effect has been reduced, as shown in Figure 13 a). By applying feedback control on the vertical acceleration measured by the IMU, the variation in thrust can be treated as a disturbance which is then controlled by a strong proportional controller.

Apparent degradation in the altitude control capabilities as forward speed increases has also been observed in flight tests. The thrust variation created by different angles of attack at varying speeds and wind conditions can have a substantial, systematic, nonlinear effect, as was derived in Section A. These effects of forward speed are strongly felt by the altitude control loop, even with the disturbance rejection provided by an integrator term. For slow changes in motion, although disturbances occur, their slow speed allows the controller to reject them effectively. However, the quadrotor is able to rapidly pitch and roll, leading to disturbances that are difficult to reject at non-zero speeds. The ability to counteract this effect in control is compounded by the difficulty of accurately measuring the ambient wind.

This is demonstrated in Figure 13 b), where the vehicle was operating under human control of attitude commands, and with the roll axis aligned with North/South. A positive roll was commanded to arrest the vehicle's sideways progress, but as it rotated through $0°$ roll while at a velocity of 3.5 m/s, the thrust increased such that the controller was unable to compensate for the upward force and caused the vehicle to "balloon" high above the commanded altitude.

C. Position Flight Control

Position control is currently implemented using a PID controller design which actuates the vehicle's roll and pitch as control inputs. Tilting the vehicle in any direction causes a component of the thrust vector to point in that direction, so commanding pitch and roll is directly analogous to commanding accelerations in the X-Y plane. Figure 14 shows a typical indoor flight using this control scheme. The vehicle is able to stay inside of a 40 cm-radius circle, which is comparable to the performance of a human operator using a joystick to actuate pitch and roll. However, the current control implementation has little ability to reject disturbances from wind and translational velocity effects. For this scale aircraft, even mild winds can cause large disturbances. A key weakness of this and similar position controllers used by other groups is the assumption that the velocity of the free stream and attitude control are decoupled. This is in fact only
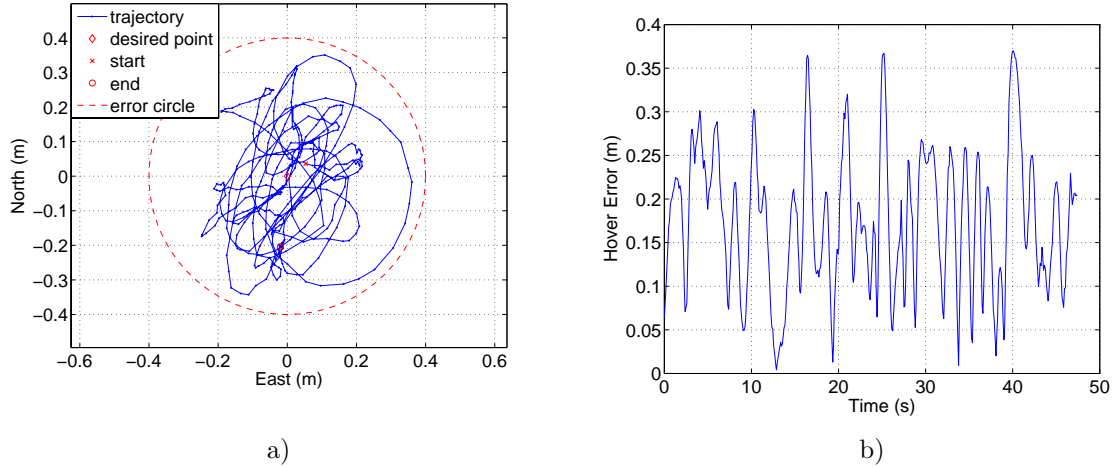
a)

b)

Figure 14. Autonomous indoor hover performance is demonstrated using an overhead camera to provide position sensing. a) Indoor hover flight with PID controller using pitch and roll commands. b) The error is kept to less than 40cm throughout the flight and is comparable to the performance of a human operator flying via joystick commands to pitch and roll.

true for very small velocities. As shown in Section V, there is significant coupling between the velocity of the aircraft and the attitude dynamics, which is to be addressed in future work as part of improved control systems design.

VII. Conclusions

Quadrotor helicopters are popular as testbeds for small UAV development, but their aerodynamics are complex and need to be accurately modeled in order to enable precise trajectory control. Although many good control results have been reported in previous work, these have focused primarily on simple trajectories at low velocities, in controlled indoor environments. In this paper, we have addressed a number of issues observed in quadrotor aircraft operating at higher speeds and in the presence of wind disturbances. We have explored the resulting forces and moments applied to the vehicle through these aerodynamic effects and investigated their impact on attitude and altitude control. We have uncovered the extent of their influence using data from static measurements and flight data from the STARMAC II quadrotor. These results have shown that existing models and control techniques are inadequate for accurate trajectory tracking at speed and in uncontrolled environments. Careful consideration of these disturbances will allow us to improve both the physical configuration and control design of the STARMAC II quadrotor, improving attitude and altitude tracking performance and permitting controlled, stable flight at higher velocities and in the presence of gusting winds. This work should open the door to improved autonomous hover and trajectory tracking in the near future, enabling most of the applications that have been envisaged for the STARMAC testbed.

Acknowledgments

American Institute of Aeronautics and Astronautics

References

[1]Hoffmann, G. M., Waslander, S. L., and Tomlin, C. J., "Distributed Cooperative Search using Information-Theoretic Costs for Particle Filters with Quadrotor Applications," *Proceedings of the AIAA Guidance, Navigation, and Control Conference*, Keystone, CO, August 2006.

[2]Stepniewski, W. Z., *Rotary-wing aerodynamics*, Dover Publications, New York, NY, 1984.

[3]Newman, S., *The Foundations of Helicopter Flight*, Halsted Press, New York, NY, 1994.

[4]Leishman, J. G., *Principles of Helicopter Aerodynamics*, Cambridge University Press, New York, NY, 2000.

[5]Prouty, R. W., *Helicopter Performance, Stability, and Control*, Krieger Publishing Company, Malabar, FL, 1990.

[6]Anderson, S. B., "Historical Overview of V/STOL Aircraft Technology," NASA Technical Memorandum 81280, Ames Research Center, Moffett Field, CA, March 1981.

[7]Altuğ, E., Ostrowski, J. P., and Taylor, C. J., "Quadrotor Control Using Dual Camera Visual Feedback," *In Proceedings of the IEEE International Conference on Robotics and Automation*, Taipei, Taiwan, Sept 2003, pp. 4294–4299.

[8]"DraganFly-Innovations DraganFlyer IV," 2006, http://www.rctoys.com.

[9]Hoffmann, G., Rajnarayan, D. G., Waslander, S. L., Dostal, D., Jang, J. S., and Tomlin, C. J., "The Stanford Testbed of Autonomous Rotorcraft for Multi Agent Control (STARMAC)," *In Proceedings of the 23rd Digital Avionics Systems Conference*, Salt Lake City, UT, November 2004.

[10]Bouabdallah, S., Murrieri, P., and Siegwart, R., "Towards Autonomous Indoor Micro VTOL," *Autonomous Robots*, Vol. 18, No. 2, March 2005, pp. 171–183.

[11]Guenard, N., Hamel, T., and Moreau, V., "Dynamic modeling and intuitive control strategy for an X4-flyer," *In Proceedings of the International Conference on Control and Automation*, Budapest, Hungary, June 2005, pp. 141–146.

[12]Escareño, J., Salazar-Cruz, S., and Lozano, R., "Embedded control of a four-rotor UAV," *Proceedings of the AACC American Control Conference*, Minneapolis, MN, June 2006, pp. 3936–3941.

[13]Nice, E. B., *Design of a Four Rotor Hovering Vehicle*, Master's thesis, Cornell University, 2004.

[14]Park, S., Won, D., Kang, M., Kim, T., Lee, H., and Kwon, S., "RIC (Robust Internal-loop Compensator) Based Flight Control of a Quad-Rotor Type UAV," *Proceedings of the IEEE/RSJ International Conference on Intelligent Robotics and Systems*, Edmonton, Alberta, August 2005.

[15]Pounds, P., Mahony, R., and Corke, P., "Modelling and Control of a Quad-Rotor Robot," *In Proceedings of the Australasian Conference on Robotics and Automation*, 2006.

[16]Castillo, P., Dzul, A., and Lozano, R., "Real-Time Stabilization and Tracking of a Four-Rotor Mini Rotorcraft," *IEEE Transactions on Control Systems Technology*, Vol. 12, No. 4, 2004, pp. 510–516.

[17]Kendoul, F., Lara, D., Fantoni, I., and Lozano, R., "Nonlinear control for systems with bounded inputs: Real-time embedded control applied to UAVs," *Proceedings of the IEEE Conference on Decision and Control*, San Diego, CA, December 2006, pp. 5888–5893.

[18]Romero, H., Benosman, R., and Lozano, R., "Stabilization and location of a four rotor helicopter applying vision," *Proceedings of the AACC American Control Conference*, Minneapolis, MN, June 2006, pp. 3930–3935.

[19]Valenti, M., Bethke, B., Fiore, G., How, J. P., and Feron, E., "Indoor Multi-Vehicle Flight Testbed for Fault Detection, Isolation, and Recovery," *In Proceedings of the AIAA Guidance, Navigation and Control Conference*, Keystone, CO, August 2006.

[20]Kroo, I., Prinz, F., Shantz, M., Kunz, P., Fay, G., Cheng, S., Fabian, T., and Partridge, C., "The Mesicopter: A Miniature Rotorcraft Concept, Phase II Interim Report," 2000.

[21]Waslander, S. L., Hoffmann, G. M., Jang, J. S., and Tomlin, C. J., "Multi-Agent Quadrotor Testbed Control Design: Integral Sliding Mode vs. Reinforcement Learning," *In Proceedings of the IEEE/RSJ International Conference on Intelligent Robotics and Systems 2005*, Edmonton, Alberta, August 2005, pp. 468–473.

[22]Mokhtari, A. and Benallegue, A., "Dynamic Feedback Controller of Euler Angles and Wind parameters estimation for a Quadrotor Unmanned Aerial Vehicle," *In Proceedings of the IEEE International Conference on Robotics and Automation*, New Orleans, LA, April 2004, pp. 2359–2366.

[23]Pounds, P., Mahony, R., Gresham, J., Corke, P., and Roberts, J., "Towards Dynamically-Favourable Quad-Rotor Aerial Robots," *In Proceedings of the Australasian Conference on Robotics and Automation*, Canberra, Australia, 2004.

[24]"Model Motors Axi 2208 Brushless Motors," http://www.modelmotors.cz/index.php?page=60&kategorie=2208.

[25]"Wattage 10×4.5 Tractor and Pusher Prop," http://www.globalhobby.com/public/gallery/131384.asp.

[26]"Castle Creations Phoenix 25 Brushless Motor Control," http://www.castlecreations.com/products/phoenix-25.html.

[27]"Microstrain 3DMG-X1 IMU," http://www.microstrain.com/3dm-gx1.aspx.

[28]"Devantech SRF08 Sonic Ranger," http://www.robot-electronics.co.uk/shop/Ultrasonic_Rangers1999.htm.

[29]"Senscomp Mini-AE Sonic Ranger," http://www.senscomp.com/minis.htm.

[30]"Novatel Superstar II GPS receiver," http://www.novatel.com/products/superstar.htm.

[31]"Gumstix Robostix microcontroller board," http://www.gumstix.com/store/catalog/product_info.php?cPath=31&products_id=139.

[32]"Crossbow Stargate 1.0 Single Board Computer," http://www.xbow.com/Products/productsdetails.aspx?sid=85.

[33]"Advanced Digital Logic ADL855 PC104+," http://www.adlogic-pc104.com/products/cpu/pc104/datasheets/MSM855.pdf.

[34]"Thunder Power Extreme Series Lithium Polymer Battery Packs," http://www.thunderpower-batteries.com/Li-PolyBatteries.htm.

[35]"Videre Design STH-MDCS 2 Stereo Vision Head," http://www.videredesign.com/sthmdcs2.htm.

American Institute of Aeronautics and Astronautics

[36] "Hokuyo URG-04LX Laser Range Finder," http://www.hokuyo-aut.jp/products/urg/urg.htm.

[37] "BackCountry Access Tracker DTS Digital Avalanche Beacon," http://www.bcaccess.com/bca_products/tracker/index.php.

[38] Franklin, G. F., Powell, J. D., and Emami-Naeini, A., *Feedback Control of Dynamic Systems*, Prentice Hall, Upper Saddle River, NJ, 4th ed., 2002.

[39] Johnson, W., *Helicopter Theory*, Princeton University Press, Princeton, NJ, 1980.

American Institute of Aeronautics and Astronautics